CLM - P 542

CLM - P 542

UKAEA

Preprint

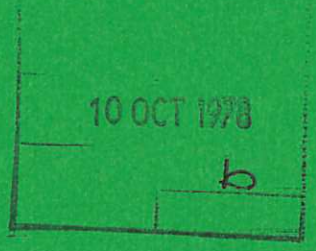

INTERPRETATION OF LINE EMISSIONS FROM HELIUM-LIKE IONS IN TERMS OF THE ELECTRON PARAMETERS AND ION DIFFUSION IN TOKAMAK PLASMAS

N J PEACOCK
H P SUMMERS

CULHAM LABORATORY
Abingdon Oxfordshire

1978

CLM-P 542

INTERPRETATION OF LINE EMISSIONS FROM HELIUM-LIKE IONS IN TERMS OF THE ELECTRON PARAMETERS AND ION DIFFUSION IN TOKAMAK PLASMAS

by

N J PEACOCK and H P SUMMERS*
Culham Laboratory, Abingdon, Oxon., OX14 3DB, UK
(Euratom/UKAEA Fusion Association)

ABSTRACT

A detailed calculation is made of the populations of the excited levels of the helium-like ion O^{+6} in a plasma, taking full account of recombination and collisional radiative processes. The results apply equally to equilibrium and non-equilibrium plasmas. Line ratios are identified which are indicative of electron temperature, electron density and the non-equilibrium state of the plasma. Useful diagnostic plots of these line ratios are given in terms of a parameter r describing the relative abundance O^{+6}/O^{+7}. Data on the electron parameters, O^{+6} line emissions and associated line emissions of O^{+5} and O^{+7} for the DITE Tokamak facility are used to test the diagnostics model. The interpretation is markedly sensitive to the electron temperature profile. The spatial variation of r from its equilibrium value allows a derivation of the helium-like ion diffusion velocity.

(Submitted for publication in J.Phys.B, Atom. Molec. Phys.)

April 1978

*Dept. of Applied Maths and Theor. Physics, University of Cambridge.
cms

NOTE

(i) The notation used in this paper to represent powers of 10 is as follows:

$$5.0^{2} \equiv 5 \times 10^{2}$$

$$2.19^{-13} \equiv 2.19 \times 10^{-13}$$

(ii) The symbol Ne is to be read as electron density (and not as neon); similarly Te is electron temperature.

1. Introduction

The motivation of this paper is two-fold. First there is a general interest in the use of measurements of line intensities from plasmas to deduce details of conditions within the plasma. We concentrate our attention on He-like ions since these are persistent over a relatively wide range of plasma parameters and are therefore common emitters in plasmas. Also extensive model calculations of the intensities of multiply-excited satellite and of intersystem lines exist for these and associated ions (Gabriel and Jordan, 1971; Gabriel, 1972). In Tokamak plasmas there is considerable scope for the use of these models on highly ionised ions such as Fe^{+24} and Ar^{+16} where the satellites and forbidden lines (e.g. $1s2p\ ^3P_1 - 1s^2\ ^1S_0$) can have an appreciable fraction of the allowed line intensities. The study of lighter elements in laboratory plasmas however, is often restricted on intensity considerations to the resonance and intercombination lines. The ranges of temperature, density and non-equilibrium state over which the ratios of He-like lines are sensitive are, of course limited and dependent upon the particular ion. The concern in this paper is with helium-like oxygen O^{+6}. The use of O^{+6} line ratios for diagnostics forms the first part of the paper.

Second there is a specific interest in the behaviour of light element impurities in the Divertor Tokamak Experiment (DITE) at the Culham Laboratory. Measurements of the photon fluxes of emission lines in the XUV region of the spectrum have been made along arbitrary chords of the small section of the torus. The n=2 and n=3 resonance lines ($2\ ^1P_1 - 1\ ^1S_0$, $3\ ^1P_1 - 1\ ^1S_0$) and the intersystem line ($2\ ^3P_1 - 1\ ^1S_0$) of O^{+6} are observed and their intensities suggest a spatially non-equilibrium plasma with an outward diffusion of the O^{+6} species from the core of the plasma. The analysis of these observations constitutes the second part of the paper.

Theoretical investigation of He-like line intensities has been carried out by a number of authors (Gabriel and Jordan, 1969; Blumenthal, Drake and

Tucker, 1972; Mewe and Schrijver, 1977) successive references corresponding to calculations of increasing refinement. The contribution of the theoretical atomic physics aspect of the present paper lies in the very full treatment of recombination and the quality of the low level cross-section data used. This part of the calculation will only be summarised here. Full details, and results for helium-like systems up to Fe^{+24} will be given in Burgess and Summers (1978 to be published).

2. Atomic Physics Model

The parameters of the plasma in the DITE Tokamak are known in considerable detail both as functions of time and space, and operating conditions (Paul et al, 1977). However in order to facilitate the line intensity model calculations we make the following general assumptions. The plasma is composed of protons, electrons and impurities and is optically thin in all spectrum lines of relevance to the present analysis. Influence of magnetic fields on the excited level populations of impurity species is neglected except in so far as they affect the mobility of the ions. The electrons and protons are assumed to be locally thermalised with the same Maxwellian temperature and the same number density. In practice (cf. section 4), there may be a 30% difference between the electron and proton concentrations and the electron and ion temperatures. These differences are not significant in our present model comparisons. Collisions between impurity species may be neglected. It should be noted that all these restrictions may be relaxed to some extent in the basic atomic physics computer codes used, the present choices being made to maintain the general applicability of the results.

2.1 Population Structure

The specific emissivites of the spectrum lines of O^{+6} are obtained immediately once the populations of the upper levels of the transitions have been calculated. These populations are required as functions of density, temperature and the ionisation state of the plasma. This last

dependence is present since in general the ionisation stages will not be in relative ionisation balance but in proportions determined by the particular transient nature of the plasma. Very many atomic processes may contribute to the population and depopulation of the excited levels of O^{+6}. These include radiative recombination, dielectronic recombination, collisional ionisation by electrons and its inverse three body recombination, excitation and de-excitation by electrons and protons and spontaneous radiative transitions between levels. In these circumstances, the definition of, for example, the effective recombination rate to a level becomes a matter of some complexity since account must be taken of all the collisional-radiative processes by which recombining electrons may circulate among other levels before reaching the specified level. A general theory applicable to this situation and special techniques for its solution have been developed (Burgess and Summers, 1969, 1976; Summers, 1977a) stimulated by the earlier work of Bates, Kingston and McWhirter (1962). These papers give the full background to the present work. Consequently only a brief description follows here.

If it is assumed that the populations of the excited levels of O^{+6} are at each moment in equilibrium relative to the instantaneous populations of the ground levels $1s^2\ ^1S_0$ and $1s\ ^2S_{\frac{1}{2}}$ of the O^{+6} and O^{+7} ionisation stages and that lower ionisation stages may be neglected, then N_σ, the population of the σ th level of O^{+6} may be written as

$$N_\sigma = U_\sigma N_e N(O^{+6}\ 1s^2\ ^1S_0) + V_\sigma N_e N(O^{+7}\ 1s\ ^2S_{\frac{1}{2}}) \qquad (1)$$

Ne is the free electron density. $N(O^{+6}\ 1s^2\ ^1S_0)$ is the abundance of the ground level of O^{+6} and $N(O^{+7}\ 1s\ ^2S_{\frac{1}{2}})$ is the abundance of the ground level of O^{+7}, these being also effectively the whole ionisation stage abundances.

$$r = N(O^{+6}\ 1s^2\ ^1S_0) \ / \ N(O^{+7}\ 1s\ ^2S_{\frac{1}{2}}) \qquad (2)$$

specifies the non-equilibrium state of the plasma. U_σ and V_σ are coefficients depending only on the temperature and density in the plasma. They correspond respectively to the effective contributions to the populations of the σth level from excitation from the ground level and from recombination and each takes account of all the indirect collisional radiative processes. Equation 1 neglects contributions to N_σ from lower ionisation stages by inner shell ionisation or multiple ionisation. This will lead to some error in transiently ionising plasmas. It is examined more fully for the DITE plasma in section 5.1. Inclusion of these effects will of course leave U_σ and V_σ unchanged. U_σ and V_σ are required for levels of the n=2 and n=3 principal quantum shells here.

In practice, the calculation of U_σ and V_σ is a very large task. The levels of the O^{+6} ionisation stage are divided into two groups, namely low levels with principal quantum number $n \leq 3$ and high levels with principal quantum number $n > 3$. The following points are of importance.

(a) For the low levels, statistical relative populations of the fine structure levels of the same LS term should not be assumed. LSJ classification of the levels is necessary.

(b) The accuracy of U for the low level populations is directly dependent on the accuracy of the rate coefficients between the low levels.

(c) High levels belonging to the same term may be assumed to be relatively statistically populated since this is preserved approximately by recombination and cascade. In addition collisional transitions tend to produce relative statistical population of high levels.

A full treatment of the recombination and population structure of LS terms including effectively an infinite number of excited states has been given by Summers (1977a). This treatment describes the high term popul-

ations and recombination satisfactorily for the present work, but does not maintain the LSJ picture detail required for the low levels. On the other hand, the statistical balance equations for the low LSJ level populations neglecting recombination and coupling to higher levels are readily established. These two aspects of the calculation may be combined in the following way. The 'condensed matrix' (Burgess and Summers, 1976) of the LS resolved population structure codes are modified by deleting rates between the low LS terms. The matrix is then reinverted and the sub-matrix corresponding to the low LS terms further inverted to yield generalised collisional dielectronic recombination, ionisation and cross-rate coefficients between the low LS terms neglecting all the direct couplings. These generalised rate coefficients may then be expanded into rates for the low LSJ levels in proportion to statistical weights and combined with the low LSJ statistical balance equations which neglect high levels. Further partial inversion yields U_σ and V_σ for the low levels.

The algebra may be summarised as follows. Let indices ρ, σ refer to the low LSJ levels, $\underline{\rho}$, $\underline{\sigma}$ refer to low LS terms, i, j refer to high LS terms and a, b refer to the totality of LS terms and spin system resolved principal quantum shells. The condensed collisional dielectronic matrix omitting coupling between low LS terms may be partitioned as

$$[C_{ab}] = \left[\begin{array}{c|c} C_{\underline{\rho\sigma}} & C_{\underline{\rho}j} \\ \hline C_{i\underline{\sigma}} & C_{ij} \end{array}\right] \qquad (3)$$

where $C_{\underline{\rho\sigma}} = 0$ for $\underline{\rho} \neq \underline{\sigma}$ is imposed.

The statistical balance equations for the LS term populations omitting couplings between low LS terms are then

$$C_{ab}\, N_b = N_e\, N_+\, r_a \qquad (4)$$

where r_a denotes recombination to the term a, and summation convention is used. Note the $N_1 = N(O^{+6}\ 1s^2\ {}^1S_0)$ and $N_+ = N(O^{+7}\ 1s\ {}^2S_{\frac{1}{2}})$. Eliminating the N_i

$$B_{\underline{\rho\sigma}}\ N_{\underline{\sigma}} = Ne\ N_+\ R_{\underline{\rho}} \tag{5}$$

where $[B_{\underline{\rho\sigma}}] = [A_{\underline{\rho\sigma}}]^{-1}$, $[A_{\underline{\rho\sigma}}] = [[C_{ab}^{-1}]_{\underline{\rho\sigma}}]$, $R_{\underline{\rho}} = \frac{1}{N_e\ N_+} B_{\underline{\rho\sigma}}\ N_{\underline{\sigma}}^{eq}$ and $N_{\underline{\sigma}}^{eq}$ denote the equilibrium populations.

Put

$$\begin{aligned} R_\rho &= \frac{\omega_\rho}{\omega_{\underline{\rho}}}\ R_{\underline{\rho}} \\ B_{\rho\sigma} &= \frac{\omega_\rho}{\omega_{\underline{\rho}}}\ B_{\underline{\rho\sigma}} \qquad \underline{\rho} \neq \underline{\sigma} \\ B_{\rho\sigma} &= 0 \qquad \underline{\rho} = \underline{\sigma}\ ,\ \rho \neq \sigma \\ B_{\rho\rho} &= B_{\underline{\rho\rho}} \end{aligned} \tag{6}$$

where the ω_ρ are the level statistical weights corresponding to the term statistical weight ω_ρ. Then the low level statistical equations become

$$E_{\rho\sigma}\ N_\sigma = N_e N_+ R_\rho \tag{7}$$

where $[E_{\rho\sigma}] = [B_{\rho\sigma}] + [D_{\rho\sigma}]$ and $[D_{\rho\sigma}]$ is the low level statistical balance matrix neglecting higher levels

Equations 7 may be rewritten as

$$E_{\rho\sigma}\ N_\sigma + E_{\rho 1}\ N_1 = N_e N_+ R_\rho \tag{7a}$$

for $\rho \neq 1$ and where the summation index σ does <u>not</u> take the value 1.

$$\frac{N_\sigma}{N_e} = \left(-\frac{E_{\sigma\rho}^{-1}\ E_{\rho 1}}{N_e}\right) N_1 + (E_{\sigma\rho}^{-1}\ R_\rho) N_+ \tag{8}$$

Hence $$U_\sigma = - \frac{E^{-1}_{\sigma\rho} E_{\rho 1}}{N_e}$$

and $$V_\sigma = E^{-1}_{\sigma\rho} R_\rho$$

2.2 Low Level Atomic Data

As mentioned in section 2.1, it is important to use the best available rate coefficient data for the low levels. The following spontaneous emission rate coefficients for O^{+6} have been used. $A(2^3S_1-1^1S_0) = 1.04^3$ sec^{-1} (Drake, 1971), $A(2^3P_1-1^1S_0) = 5.53^8$ sec^{-1}, $A(2^1P_1-2^1S_0) = 6.41^4$ sec^{-1} (Drake and Dalgarno, 1969), $A(2^3P_2-1^1S_0) = 3.34^5$ sec^{-1}, $A(2^3P_1-2^3S_1) = 8.05^7$ sec^{-1}, $A(2^3P_2-2^3S_1) = 8.20$ sec^{-1} (Blumenthal, Drake and Tucker, 1972), $A(2^1S_0-1^1S_0) = 2.31^6$ sec^{-1} (Drake, Victor and Dalgarno, 1970), $A(2^1P_1-1^1S_0) = 3.31^{12}$ sec^{-1} (Dalgarno, 1971), $A(2^3P_0-2^3S_1) = 7.993^7$ sec^{-1}, $A(2^1P_1-2^1S_0) = 2.602^7$ sec^{-1} (UCL). The UCL results indicate our own calculations using the multiconfiguration bound structure codes developed at University College, London (Eissner, Jones and Nussbaumer, 1974). These codes are based on a scaled Thomas-Fermi potential and incoporate Breit-Pauli relativistic corrections. For the n=3 levels, only dipole transition probabilities are included and these are calculated using the UCL codes. The UCL values serve as a check and for comparison with the values of Dalgarno, Drake and coworkers. Comparison is possible for electric dipole, electric quadrupole and magnetic dipole transition probabilities. Agreement is within 5% for all cases except $A(2^3P_1-1^1S_0)$ for which the UCL value is 30% smaller and $A(2^1P_1-2^3S_1)$ for which the UCL value is 16% smaller.

Magee, Mann, Mertz and Robb (1977) have compiled a large amount of electron collision strength data for O^{+6}. This has proved most useful for the present work. For transitions between the n=1 and 2 shells and within the n=2 shell, the most sophisticated collision strength calcul-

ations are the close coupling results of Robb and the distorted wave results of Norcross. These provide a useful contrast since the Robb calculation treats the collision in considerable refinement but uses a relatively simple target state, while the Norcross calculation treats the collision more simply but uses a complex target. The results of Robb are usually larger than those of Norcross varying between 5% and 50% at threshold and of course becoming similar at high energy. In particular at threshold for the 1^1S_0-2^1P_1 collision strength, Robb is 30% greater than Norcross while for the 1^1S_0-2^3P_1 collision strength, Robb is 3% greater than Norcross. We have adopted the Norcross values in this work for the following reasons. The Norcross target states are the same as the bound states used in the UCL spontaneous coefficient results of the last paragraph. The UCL spontaneous coefficients agree closely with the results of Dalgarno, Drake and coworkers and also with the values given in Weise, Smith and Glennon (1966) so giving confidence in the target states. Recent evidence seems to suggest that a sophisticated target state is most important in computing high accuracy collision strengths. In assessing the sensitivity of the final results of this paper, however, we view the difference between the collision strengths of Norcross and Robb as indicating broadly the error bounds in the collision strengths. The electron collision strength calculations of Sampson and Parks (1974) with the prescription given in Magee et al is used for transitions involving the n=3 shell. These are Coulomb-Born calculations with uncertainties in the collision strengths near threshold $\sim$ 100%. Proton collisions are important only for transitions within a principal quantum shell. For the n=2 shell, the proton collision strengths are approximately 1/60 of the electron collision strengths and so are omitted. They are however important for the n=3 shell. Only the proton dipole collision strengths are included.

The rate coefficients used in the high level LS coupled population

structure calculation are described fully in Summers (1977a). Assessment of the accuracy of this part of the calculation is difficult since the effective recombination contributions from high levels are generally collective effects. Comparison of the most important low level individual rates where possible suggests an accuracy of better than 30%.

The dielectronic recombination rate to helium-like systems has been calculated by Burgess and Tworkowski (1976). Their original calculations provided the total low density dielectronic rate coefficient. For present purposes, the rate coefficients to individual levels are required. The codes have been modified and re-executed to provide these. At the same time an error in the treatment of the radiative stabilisation has been corrected. This does not produce a significant change in the total coefficient, but is important for the individual components. It should be noted that the results on the dielectronic rate take account of configuration mixing in the doubly excited resonant states, and in particular the mixing of the form 2snl, 2pnl±1. The details of the calculation show this to be of considerable importance.

3. Indicator Plots

Tabulations of U and V for the 2^1P_1, 2^3S_1, 2^3P_1 and 3^1P_1 levels of O^{+6}, Ne^{+8}, Mg^{+10}, Si^{+12}, S^{+14}, A^{+16}, Ca^{+18} and Fe^{+24} will be given in Burgess and Summers (1978 - to be published), for a range of electron temperatures and densities. On considering the ratios of the emissivities of particular lines, it is found that for certain ranges of electron temperature Te, electron density Ne and non-equilibrium parameter r, $I(2^3P_1-1^1S_0)/I(2^1P_1-1^1S_0)$ is sensitive to r, $I(2^3S_1-1^1S_0)/I(2^1P_1-1^1S_0)$ is sensitive to Ne and $I(3^1P_1-1^1S_0)/I(2^1P_1-1^1S_0)$ is sensitive to Te, all these ratios being more weakly dependent on the other parameters. It is therefore possible to present diagnostic indicator plots which exploit these sensitivities. For a specified electron temperature, the plot of $I(2^3S_1-1^1S_0)/I(2^1P_1-1^1S_0)$ against $I(2^3P_1-1^1S_0)/$

$I(2^1P_1-1^1S_0)$ for $0 \leq r < \infty$ and 1.0^8 cm$^{-3} \leq$ Ne $\leq 1.0^{14}$ cm^{-3} expands well over the co-ordinate space with lines of constant r and constant Ne nearly orthogonal over a substantial region. The plot is dependent on Te. Figures 1, 2, 3 and 4 give such plots for a set of temperatures spanning the range of interest for the DITE Tokamak. Some features are of interest. The ionisation equilibrium line lies close to the r=∞ boundary where the r lines accumulate. It is evident therefore that the diagnostic plot is not a sensitive indicator of r for a plasma which is ionising or near ionisation equilibrium, but is good for a recombining plasma. Likewise the plot is a good indicator of Ne in the range 1.0^{10} cm$^{-3} \leq$ Ne $\leq 1.0^{12}$ cm^{-3}, but is less sensitive for Ne > 1.0^{12} cm^{-3}. The Tokamak plasma unfortunately falls in this latter range. O^{+6} is not useful for density diagnostics at Tokamak densities. In population structure calculations the electron density Ne scales approximately as z_1^7 where z_1-1 is the ion charge. This suggests that Si^{+12} might prove a useful density indicator for Tokamaks.

For a fixed electron density, the plot of $I(3^1P_1-1^1S_0)/I(2^1P_1-1^1S_0)$ against $I(2^3P_1-1^1S_0)/I(2^1P_1-1^1S_0)$ for $0 \leq r < \infty$ and 1.0^6 K $\leq$ Te $\leq 1.0^7$ K again shows reasonable sensitivity. This plot is only weakly dependent on Ne and so figure 5 for the single electron density 1.0^{13} cm^{-3} is adequate for derivation of Te and r for the range of density likely to be encountered in Tokamak devices.

If the four spectrum lines mentioned are observable, then from the two types of diagnostic plot (i.e. those shown in figures 1-4 and that shown in figure 5) Te, Ne and r may be determined. If Te and Ne are known tentatively, then the plots provide r and a consistency check. Alternatively, if, as is often the case in Tokamak research, Te and Ne are known accurately as a function of space and time then the plots may be used to investigate the theoretical collision strength data. From the point of view of deriving atomic rate coefficients, Tokamak plasma studies could prove invaluable. The temperature determination from figure 5 is sensitive to the $1^1S_0-2^1P_1$ and $1^1S_0-3^1P_1$ collis-

ion strengths. This is discussed further in section 5.1.

4. Spectroscopy on DITE

The DITE Tokamak, in common with many present-day Tokamaks, is capable of stable operation with electron densities in the range $10^{13} \leq Ne \leq 10^{14}$ cm^{-3} and electron temperatures in the range 0.2 to 1 keV. These limits are quoted here only as a guide and may be overly restrictive when applied to the wide variety of operating parameters in DITE. A summary of the operational characteristics and performance of DITE has been given by Paul et al. (1977).

For the purposes of the present spectroscopic data, DITE was operated with a 100 kA ohmic heating current, with the current limiter aperture at a radius of 26 cm and with a main stabilising toroidal magnetic field of 1.3 Tesla. No additional heating by particle beam injection or improvements to the purity of the plasmas by gettering or gas injection during the current pulse, were involved.

Spectra in the range 10 to 300 Å were photographed on SC5 plates with a 2 metre grating spectrograph (model E580 supplied by Rank Precision) fitted with a 1200 line/mm ruled grating, and with the light incident at a grazing angle of 2^{o}. The central 125 msec of each 250 msec current pulse was selected by mechanical shuttering. A spatial scan of the plasma emission was performed with an incremental step of 3 cm in the radius on a shot by shot basis. Typically the plate corresponding to each radial position was exposed to about seven discharges and every effort was made to keep the plasma parameters reproducible during the total radial scan of the plasma. The electron density is deduced from multichannel microwave data, and the electron temperature from measurements of Thomson scattering of light from a ruby laser. In retrospect it was realised that the radial distribution of the temperature can vary from discharge to discharge, while the spectroscopic data corresponds to a time average of profiles. Density and temperature profiles $Ne(\rho)$ and $Te(\rho)$ measured prior to the spectroscopic data, are shown in figure 6. In the light of subsequent analysis, the central temperature

profile Te(0) is probably an upper bound for this experiment. A reason for this is the progressive desorption of oxygen from the walls when the Tokamak is operated over a period of time. A reduced oxygen contamination at the walls actually allows a higher concentration of metal wall impurities to reach the core of the plasma. The radiation loss from metal ion impurities exceeds that from oxygen ions and can give rise to reduced, even 'hollow' central temperature profiles. (Hugill et al, 1978). Examples of these are shown in figure 6.

Analysis of the specific intensities of the line emission from the various ion species to be found in the DITE Tokamak indicates that oxygen is the most abundant impurity element. The resonance lines of O^{+7}, O^{+6} and O^{+5} are prominent spectral features in a radial scan of the emission. Microphotometer tracings are made of the photographically recorded spectra. Using previous calibrations of the spectrograph for absolute sensitivity against wavelength (Hobby and Peacock, 1973) but modified for altered slit width, grating and plate sensitivity, the data is converted into line of sight intensities.

After Abel inversion, the experimental data consists of the specific emissivities of the lines as a function of plasma radius. For the present diagnostics, only the emissivities $I(2^1P_1-1^1S_0)$, $I(3^1P_1-1^1S_0)$ and $I(2^3P_1-1^1S_0)$ for O^{+6} (denoted by I_R, $I_{R'}$ and I_I) on a relative scale are required. The forbidden line $2^3S_1-1^1S_0$ is not observed. However, $I(2^2P-1^2S)$ of O^{+7} denoted by I_α, and $I(3^2P-2^2S)$ of O^{+5}, denoted by $I_{R''}$, were also evaluated on an absolute scale. These are important in our assessment of the observations and the present models in the next section. The specific emissivities of the measured lines are shown in figure 7.

Reduction of the allowed line intensities by opacity has been considered and shown to require plasma dimensions of several tens of metres. An optically thin situation for the O^{+7}, O^{+6} and O^{+6} lines in DITE can safely be assumed.

5. Analysis of the DITE Plasma

5.1 Diagnostics

Since the forbidden line is not observed, the principal density

indicator ratio $I(2^3S_1-1^1S_0)/I(2^1P_1-1^1S_0)$ is not available and in any case would lie in the least sensitive region of figures 1, 2, 3 and 4 at the typical Tokamak densities. The ratio $I(2^3P_1-1^1S_0)/I(2^1P_1-1^1S_0)$ is available. With electron temperatures and densities obtained from figure 6, this ratio, in conjunction with figures 1, 2, 3 and 4 yields the non-equilibrium parameter r (equation 2) as a function of radius. However, since the absolute line emissivities are available, we use equations 1 directly for the resonance and intercombination lines to obtain the absolute particle densities for the O^{+6} and O^{+7} ionisation stages. For conciseness, let n_i denote the density $N_1(O^{+(Z_o-i)})$ where Z_o is the nuclear charge, and subscripts R, I and α be used for the O^{+6} resonance and intercombination lines and the O^{+7} Lyman α line respectively. I_R, I_I, U_R, V_R, U_I, V_I, n_1 and n_2 are given as functions of radius in table 1. The ratio n_1/n_2 in comparison with the values obtaining in ionisation equilibrium indicate a recombining plasma.

I_α is also given in table 1. The upper level of this transition ($O^{+7}(2p)$) is populated by excitation from the ground level of O^{+7} and by recombination from O^{+8}. Excitations to the 2s and 2p levels will both lead to O^{+7} Lyman α emission since the 2s level is metastable and electron and proton collisions rapidly redistribute electrons between the 2s and 2p levels at Tokamak densities. There is no dielectronic recombination to O^{+7} levels, and so, even if it is assumed that the O^{+8} stage is fairly strongly recombining, the preponderance of O^{+7} Lyman α radiation will be due to excitation. If it is assumed that the whole intensity I_α arises from excitation to 2s and 2p, then we may deduce a close upper bound n_1^* to the stage density n_1. Using the initial, time averaged temperature profile showing a central peak in figure 6, the results of the analysis are shown in table 1. The collision strengths used are the close-coupling results of Robb (Magee et al, 1977) and should be of high reliability. Comparison of n_1 and n_1^* indicates major disagreements, with

differences varying between 10 and 20 times. In attempting to resolve this discrepancy we have examined three possibilities.

(a) Suppose that, instead of being transiently recombining, the plasma is in fact strongly transiently ionising. In such a situation inner shell ionisation of O^{+5} could be significant. Further, although the cross-sections for inner shell ionisation of O^{+5} leaving the target in excited states of O^{+6} are unknown, it is probable that relative contributions to triplet and singlet populations will be approximately statistical. This would lead to enchancement of the intercombination line over the resonance line similar to that in the recombining plasma. The resonance line 3^2P-2^2S of O^{+5}, ($I_{R''}$ in figure 7) is observed. An upper bound to the stage density n_3 may be deduced by assuming that excitation is the sole mechanism leading to this line emission. Consequently an upper bound to the inner shell ionisation contribution of the O^{+5} state to the $O^{+6}(2^3P_1)$ level may be obtained by assuming that the whole inner shell ionisation rate leads to population of the 2^3P_1 level. Using the excitation cross-section data of Robb (Magee et al, 1977) and the ECIP approximation for the ionisation cross-section (Burgess and Summers, 1976; Burgess, Summers, Cochrane and McWhirter, 1977), it is found that the O^{+5} stage contribution is negligible (less than 1% of the total at all radial positions through the plasma).

(b) We next consider the variation possible in the theoretical predictions due to uncertainty in the atomic data. Comparative assessment of the collision strength data for O^{+6} has been given in section 2.2. We note that the threshold differences in the collision strength are overly pessimistic for the rate coefficients. Robb and Norcross collision strengths move into close agreement quite quickly above threshold. On integrating over a Maxwellian electron distribution, maximum differences in the rate coefficients are about 10%. Hence the maximum uncertainty in the most critical rate coefficients can not reasonably be put at greater

than about 20%. If this maximum variation was expressed entirely in an increase or decrease in the 1^1S_0-2^1P_1 excitation rate coefficient, then the variation in n_1 and n_2 is about 35%. Recombination contributions are dominated at the higher temperatures by dielectronic recombination. As described in section 2.2, the most recent results of Burgess and Tworkowski are used for this process. The authors give a correction to the older 'general formula' (Burgess, 1965) estimates. For total dielectronic recombination to O^{+6} the new results are approximately 65% of the old values. Also we have neglected all core excitations other than the 1s-2p. The total dielectronic rate therefore is approximately 50% of the value used in the ionisation balance calculation of Summers (1974). Most pessimistically, suppose that the recombination contributions could be increased by a factor 2. Then the estimate of n_1 would be decreased by about the same factor. We conclude that reasonable variation in the theoretical data cannot accommodate the entire discrepancy between n_1 and n_1^*.

(c) It seems therefore that the large variation between n_1 and n_1^* and the differential variation across the Tokamak may have its origins in the effective electron temperature. This may be clarified as follows. Suppose that the procedure for deducing n_1 from I_α is correct. Then equations 1 for the resonance and intercombination lines yield a consistency relation for the electron temperature. That is we seek the temperature $\overline{Te}$ for which

$$\frac{I_I}{I_R} - \frac{A_I\ U_I}{A_R\ U_R} - \frac{I_\alpha\ A_I}{I_R\ q_\alpha}\left(V_I - \frac{V_R\ U_I}{U_R}\right) \qquad (9)$$

is zero. In this expression, q_α denotes the effective excitation rate coefficient to the O^{+7} (^2P) term. A_R and A_I are the Einstein coefficients

for the resonance and intercombination lines of O^{+6} respectively. $\overline{Te}$ is plotted as a function of radius in figure 6 for comparison. $\overline{Te}$ and $\overline{n}_1/\overline{n}_2$ are tabulated in table 2. The central temperature estimate is approximately 50% of the Thomson scattering peaked central temperature, measured at the beginning of the experiment, the difference becoming less towards the plasma periphery. Also a slight temperature rise at a radius of 8 cm is evident. Note that because of the smallness of the I_α intensity towards the plasma periphery, the revised electron temperature will have large uncertainties in that region. In the light of this theoretically revised temperature, the experimentally determined temperature profile has been reconsidered. The temperature profile $Te(\rho)$ of figure 6 is composed from samples taken at 60 msec. after initiation of the current pulse, and with the limiter at 26 cm. Examination of some individual profiles taken in conjunction with the spectroscopic data indicate that the temperature profile evolves during the current pulse, showing sometimes a decreasing central temperature with time. Two typical temperature profiles for the 26 cm limiter position at 60 msec and 120 msec are shown in figure 6. The peaked central profile $Te(\rho)$ therefore should be considered an upper bound for this experiment. We note also the uncertainties in the Abel inversion of data. To summarise, there are good grounds for a lower effective electron temperature for O^{+6} line formation in the plasma, however, the inclusion of the peaked $Te(\rho)$ profile serves to indicate, section 5.2, the sensitivity of the diffusion analysis to the actual temperature profile to be associated with the spectroscopic cata.

The electron temperature may also be deduced from the temperature diagnostic (figure 5). The theoretical emissivity $I(3^1P_1-1^1S_0)$ of O^{+6} is dependent on the collision strength $1^1S_0-3^1P_1$. Also it is the threshold region of the collision strength which is of most importance, and there, elaborate resonant structure is to be expected. The expression of Sampson and Parks (1972) used here takes no account of such structure, hence the

large uncertainty $\sim$ 100% at threshold. Such a variation in the 1^1S_0-3^1P_1 collision strength gives a larger variation in the predicted temperature. Thus the ab initio predictive value of the temperature diagnostic is severely limited by uncertainties in the collision strength data. However, a revised collision strength for 1^1S_0-3^1P_1 may be deduced from the observed emissivity (I_R, in figure 7) and the peak temperature profile $Te(\rho)$ together with the stage abundances n_1 and n_2 obtained earlier. We express this as a scaling factor F for the 1^1S_0-3^1P_1 collision strength. A value of F is obtained therefore at each radial position across the plasma. Likewise I_R', $\bar{n}_1$, $\bar{n}_2$, and the theoretically revised temperature $\bar{Te}$ may be used to deduce a scaling $\bar{F}$. Both F and $\bar{F}$ vary through the plasma being approximately 2 in the centre and 1 in the periphery. Averaging the values of F and $\bar{F}$ across the plasma yields 1.42 ± 0.55 and 1.55 ± 0.49 respectively. Neither temperature profile is favoured by this result, the variances in the two cases being similar. The close agreement between F and $\bar{F}$ is surprising and arises from the balance between non-equilibrium state and temperature. In view of this agreement, we give a revised temperature diagnostic plot (figure 8) obtained by scaling up the 1^1S_0-3^1P_1 collision strength by the factor 1.5.

5.2 Diffusion Velocities

The longevity of the Tokamak plasma suggests that the observations of the emissivities $I(2^1P_1\text{-}1^1S_0)$ and $I(2^3P_1\text{-}1^1S_0)$ (I_R and I_I in figure 7) may be interpreted as due to the diffusion of the O^{+6} species radially outwards from the hot core of the plasma. The analysis is entered therefore with the following assumptions.

(a) The plasma is static in time but spatially non-equilibrium.

(b) The plasma has cylindrical symmetry in the small section of the torus.

Let v_i denote the diffusion velocity of the $O^{+(Z_o-i)}$ species, S_i denote the collisional dielectronic ionisation rate coefficient from the stage

$O^{+(Z_o-i)}$ and α_i denote dielectronic recombination rate coefficient to the stage $O^{+(Z_o-i)}$, the stage density being n_i as before. The present objective is to deduce a diffusion velocity for the O^{+6} species without inquiring into the origin of this velocity, be it in the field, thermal or concentration gradients in the plasma. Let ρ denote the radial co-ordinate in the small section of the torus. The diffusion equations for the O^{+7} and O^{+6} ionisation stages are

$$\frac{1}{Ne}\frac{1}{\rho}\frac{d}{d\rho}\ (\rho v_1 n_1) = \alpha_1 n_o - (\alpha_2 + S_1)n_1 + S_2 n_2 \qquad (10)$$

$$\frac{1}{Ne}\frac{1}{\rho}\frac{d}{d\rho}\ (\rho v_2 n_2) = \alpha_2 n_1 - (\alpha_3 + S_2)n_2 + S_3 n_3 \qquad (11)$$

Equation 11 may be solved for the diffusion velocity v_2, equation 10 yielding only a constraint on the velocity v_1 and abundance n_o. Expressing equation 11 in difference form by setting $\rho = sh$, with h the radial interval, and putting $v_2 = 0$ at $\rho = 0$.

$$v_2(sh).n_2(sh) = \frac{h}{s}\left[\tfrac{1}{4}\omega(0) + \sum_{k=1}^{s-1} k\omega(kh) + \frac{(2s-1)}{4}\omega(sh)\right] + O(h^2) \qquad (12)$$

where

$$\omega = \alpha_2 n_2 Ne \left[\left(\frac{n_1}{n_2}\right) - \left(\frac{n_1}{n_2}\right)^{eq} - \left(\frac{\alpha_3}{\alpha_2}\right) + \left(\frac{S_3 n_3}{\alpha_2 n_2}\right) \right] \qquad (13)$$

The solution may be obtained for the temperature profiles Te and $\overline{Te}$. n_1, n_2 and n_3 or alternatively $\overline{n}_1$, $\overline{n}_2$ and $\overline{n}_3$ were deduced in section 5.1. α_2, α_3 and $\left(\frac{n_1}{n_2}\right)^{eq}$ (the ionisation equilibrium abundance ratio) may be obtained from the tabulations of Summers (1974, 1977b), and likewise the 'barred' quantitaties for the $\overline{Te}$ profile. Table 2 shows v_2 and $\overline{v}_2$

together with the intermediate data composing the source function ω.

Consider first the results for the temperature profile Te. A nearly constant outward diffusion velocity for the O^{+6} species is obtained. The non-equlibrium ratio $\left(\frac{n_1}{n_2}\right)$ dominates the source function, the difference between $\left(\frac{n_1}{n_2}\right)$ $\left(\frac{n_1}{n_2}\right)^{eq}$ indicating strong recombination from the O^{+7} to O^{+6} stage. Comparison of $\left(\frac{\alpha_3}{\alpha_2}\right)$ $\left(\frac{S_3 n_3}{\alpha_2 n_2}\right)$ indicates that the O^{+5} stage is recombining towards the centre of the plasma and ionising towards the periphery. The overall picture is insensitive to the atomic data.

For the profile $\overline{Te}$ the situation is reversed. A fairly slow inward diffusion of the O^{+6} species is found. Also over most of the plasma O^{+7} is recombining to O^{+5}. We note that in this case, the results are quite sensitive to the atomic data. Uncertainties of 100% in the collisional dielectronic coefficients are possible. Such variations are sufficient to change stages from recombining to ionising in certain regions of the plasma. Inward diffusion is obtained since accumulation of O^{+6} by recombination from O^{+7} is exceeded by depletion due to recombination of O^{+5} from O^{+6}. From a global viewpoint, the results for the profile $\overline{Te}$ are confusing. However we note that the strong evidence for time transient recombination in the plasma indicates that premise (a) of this subsection is invalid. A negative time partial differential should be present in equation 11 tending to reverse the diffusion direction.

6. Conclusions

Detailed calculations of the population of excited levels in helium-like O^{6+} and of the intercombination and allowed resonance line intensities have been made for a wide range of plasma parameters and in terms of the ratio of the ground state populations of O^{6+} and O^{7+}.

It is proposed that simple local measurements of the relative intensities of the strong helium-like lines can be used to derive the electron parameters and the non-equilibrium state of the ion species. No absolute calibration of

the detection system is required.

Full validation of the procedures in the DITE Tokamak facility has been attempted. It has been shown that interpretation of the laboratory data is very sensitive to the electron temperature. Our analyses using data from DITE Tokamak indicates that a peaked central electron temperature profile measured by Thomson scattering at the outset of the experiment is inconsistent with the results of the spectroscopic analysis. The theoretical model agrees with a hollow central temperature profile more commonly observed in the later phase of the experimental programme. An accurate quantitative assessment is inhibited by inadequate data on the electron temperature profile and to a lesser extent by some uncertainties in the theoretical atomic data. The experimental results suggest an upward revision of the theoretical cross-section used for the excitation $1^1S_0-3^1P_1$. Inferred ion diffusion velocities $\gtrsim 10^4$ cm sec^{-1} are also sensitive to the temperature profile.

It is likely that the various discrepancies revealed in the paper have their origin in the temporal variation of the plasma parameters. We anticipate further investigation of the helium-like lines with time resolved data, possibly taking account also of the finite lifetimes of the helium-like metastable levels.

Acknowledgements

We wish to acknowledge our collaboration with the DITE group in this study. M G Hobby provided the basic spectroscopic data and R Prentice the electron parameter data. We would also like to thank Dr R W P McWhirter and Dr A Burgess for numerous helpful discussions. Dr A Burgess provided the computations of the dielectronic rate coefficients and Dr D Norcross kindly provided additional cross-section data in advance of publication.

References

Bates, D R, Kingston, A E and McWhirter, R W P (1962) Proc. R. Soc., A267, 297

Blumenthal, G R, Drake, G W F and Tucker, W H (1972) Astrophys.J, 172, 205

Burgess, A (1965) Astrophys.J, 141, 1588

Burgess, A and Summers H P (1969) Astrophys.J, 157, 1007

Burgess, A and Summers H P (1976) Mon.Not.R. astr. Soc, 174, 345

Burgess, A, Summers, H P, Cochrane, D and McWhirter R W P (1977) Mon.Not.R.astr. Soc, 179, 275

Burgess, A and Tworkowski, A A (1976) Astrophys.J, 205, L105

Dalgarno, A (1971) Proc. Menzel Symp. on solar phys, atomic spectra and gaseous nebulae, NBS Special pub. no. 353

Drake, G W F (1971) Phys. Rev., A3, 908

Drake, G W F and Dalgarno, A (1969) Astrophys. J, 157, 459

Drake, G W F, Victor, G A and Dalgarno, A (1969) Phys. Rev., 180, 25

Eissner, W, Jones, M and Nussbaumer, H (1974) Comp.Phys. Commun., 8, 270

Gabriel, A H (1972) Mon.Not.R. astr. Soc., 160, 99

Gabriel, A H and Jordan, C (1971) 'Case Studies in Atomic Collision Physics' Vol 2, chapter 4

Gabriel, A H and Jordan, C (1969) Mon.Not.R.astr.Soc., 145, 241

Hobby, M G and Peacock, N J (1973) J.Phys.B., 6, 854

Hugill, J, Fielding, S J, Gill, R D, Hobby, M G, McCracken, G M, Paul, J W M Peacock, N J, Powell, B A, Prentice, R and Stott, P E (1978) Proc. 8th Europ. Conf. on controlled fusion and plasma physics, Prague (1977), vol. 1, 39

Magee, N H, Mann, J B, Mertz, A L and Robb, W D (1977) Los Alamos Scientific Laboratory Report, LA-6691-MS

Mewe, R and Schrijver, J, (1977) Space Research Laboratory (Utrecht) preprint LRO-6

Paul, J W M, Costley, A E, Fielding, S J, Forrest, M J, Gill, R D, Hugill, J, McCracken, G M, Peacock, N J, and Stott, P E (1977) Culham Laboratory Report, CLM-P502. (To be published in the proceedings of the 8th European Conference on Controlled Fusion and Plasma Physics, Prague, 1977)

Sampson, D H and Parks, A D (1974) Astrophys.J. Supple, 28, 323

Summers, H P (1977a) Mon.Not.R.astr. Soc., 178 , 101

Summers, H P (1977b) Culham Laboratory internal document

Summers, H P (1974) Appleton Laboratory Report, IM367

Weise, W L, Snith, M W and Glennon, B M (1966) US Dept. of Commerce, 'Atomic Transition Probabilities, Vol. I', NSRDS-NBS4

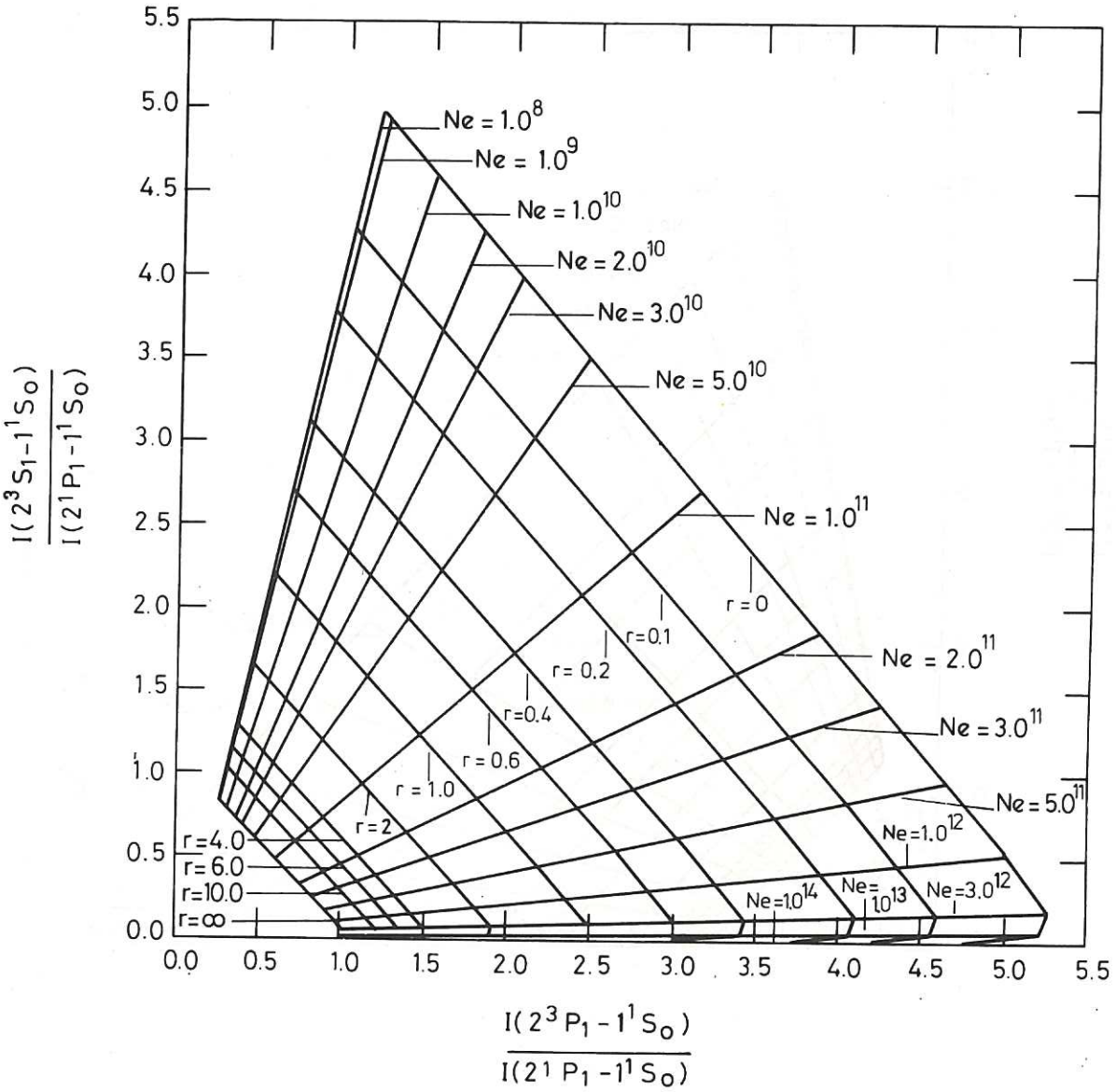

Fig.1 Ne – r diagnostic plot. Te = 10^6 K (c.g.s. units).

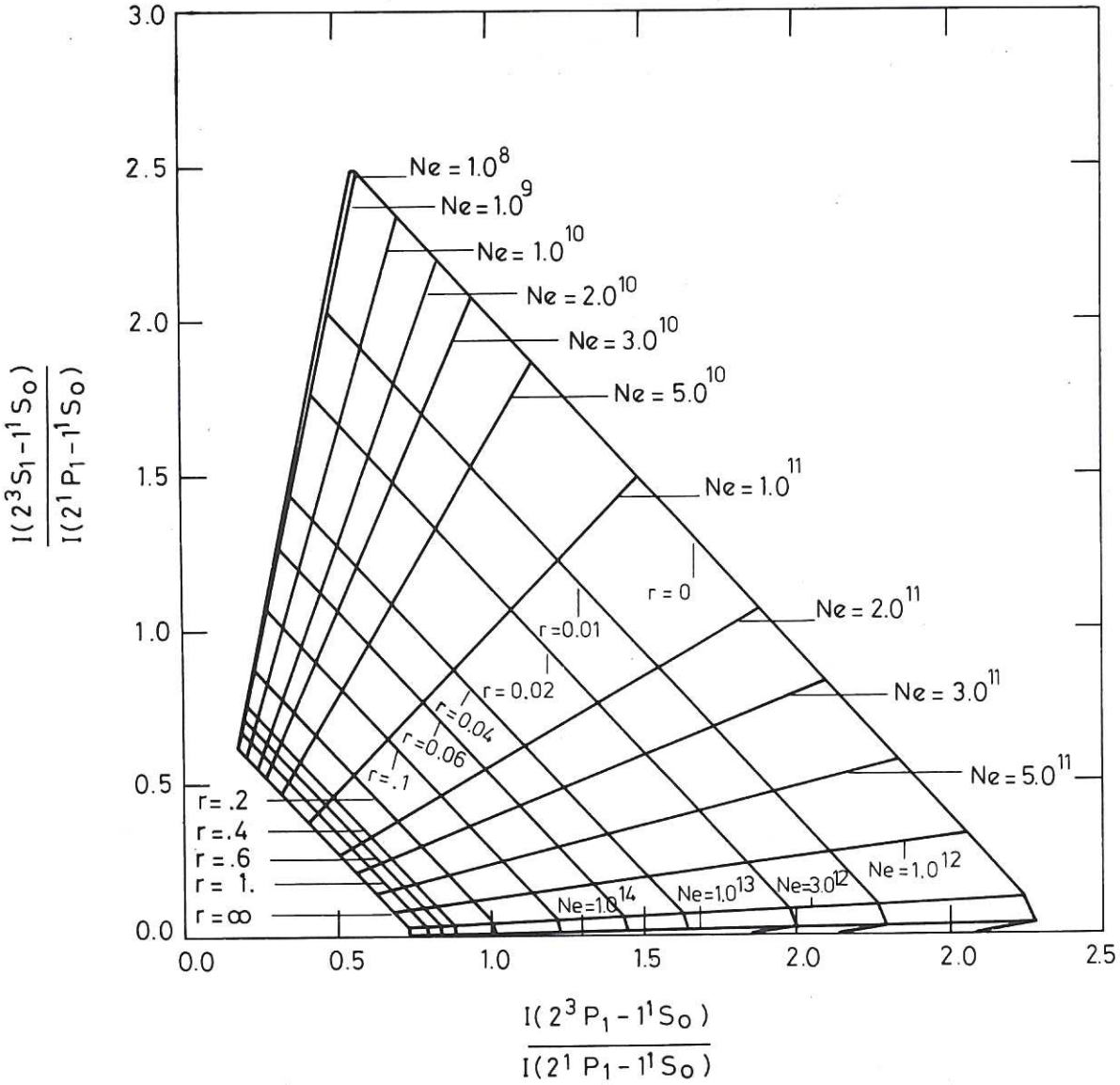

Fig.2 Ne – r diagnostic plot. Te = 2·0^6 K.

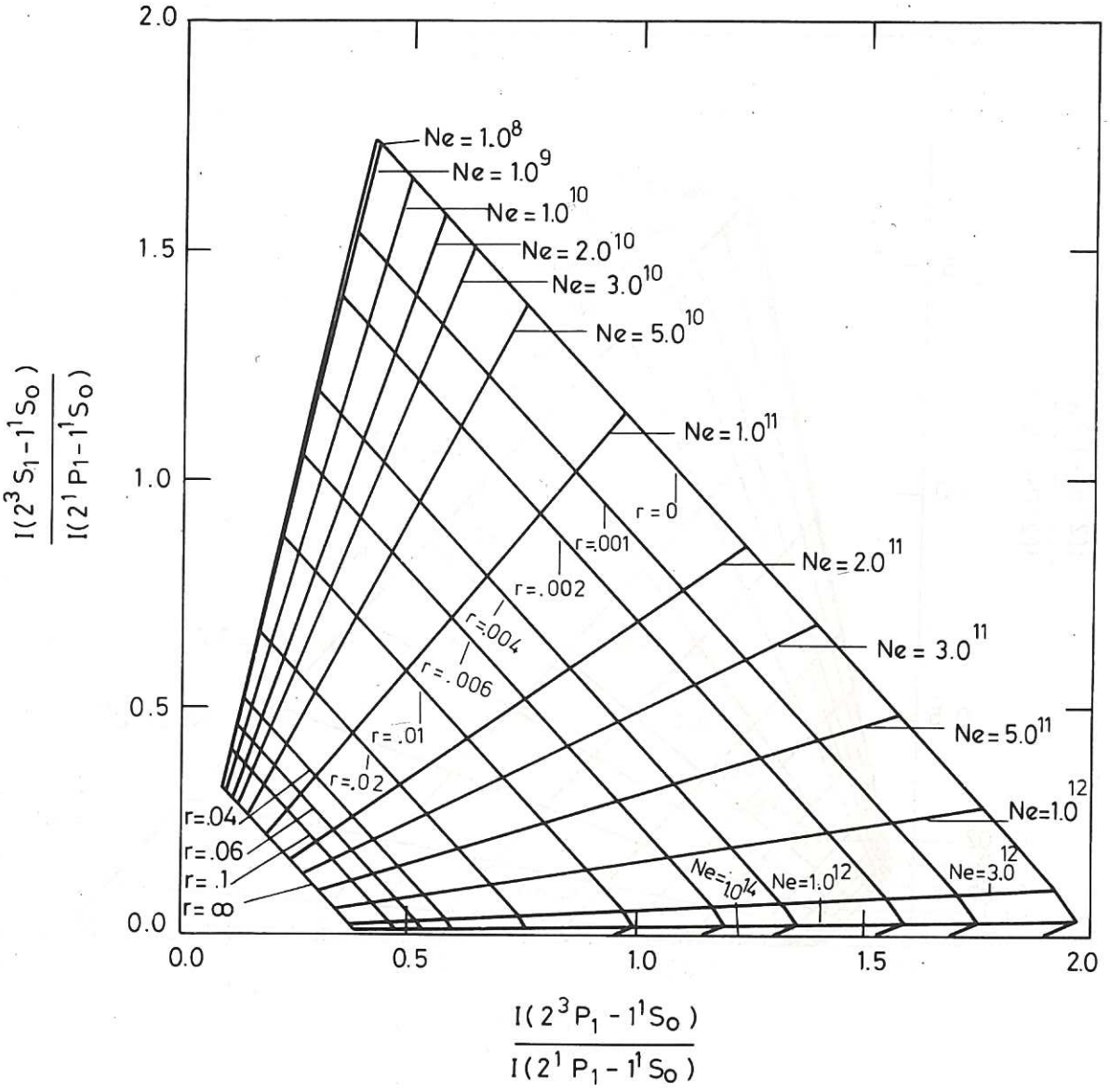

Fig.3 Ne – r diagnostic plot. Te = 5·0^6 K.

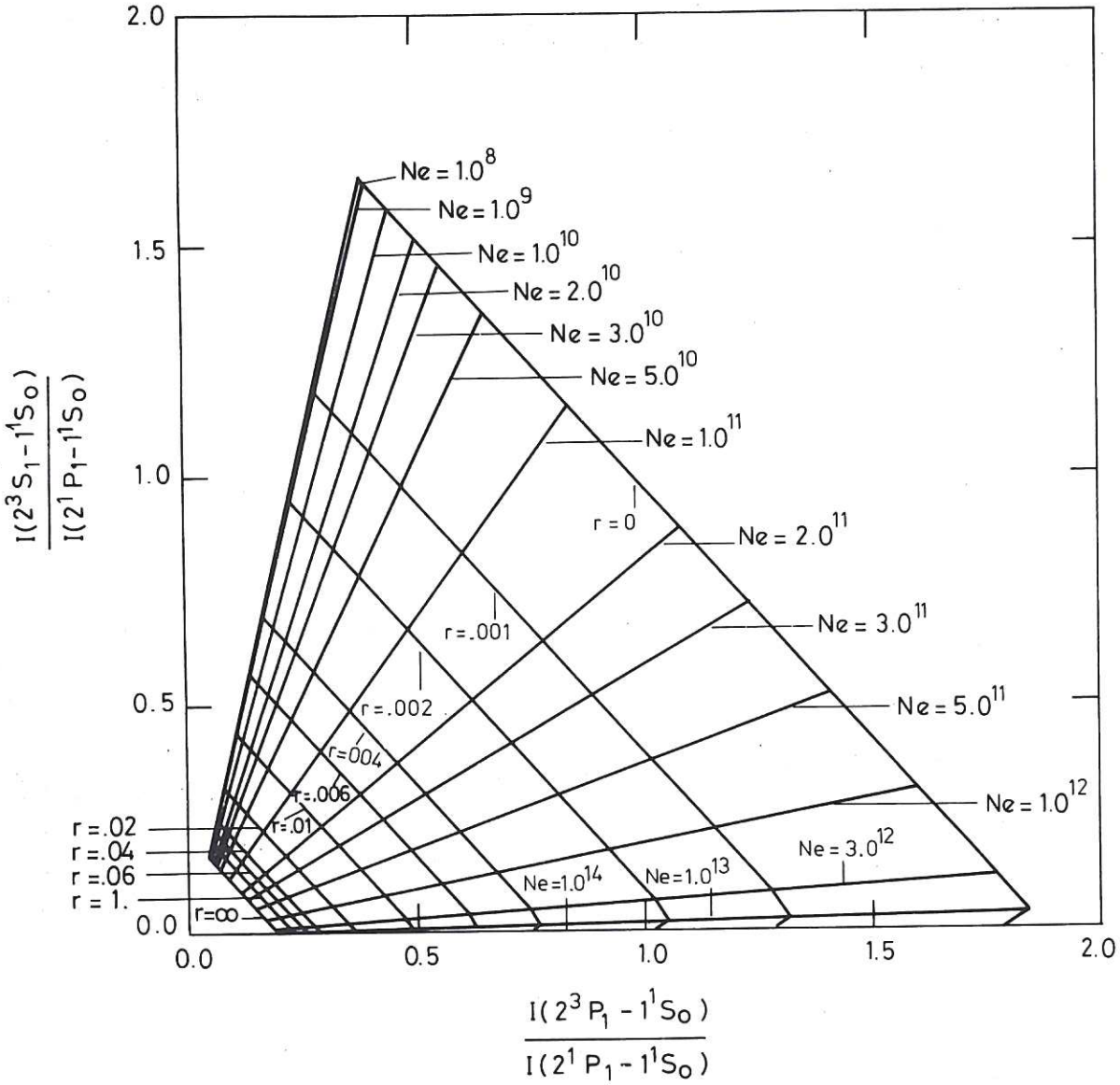

Fig.4 Ne – r diagnostic plot. Te = 1·0^7 K.

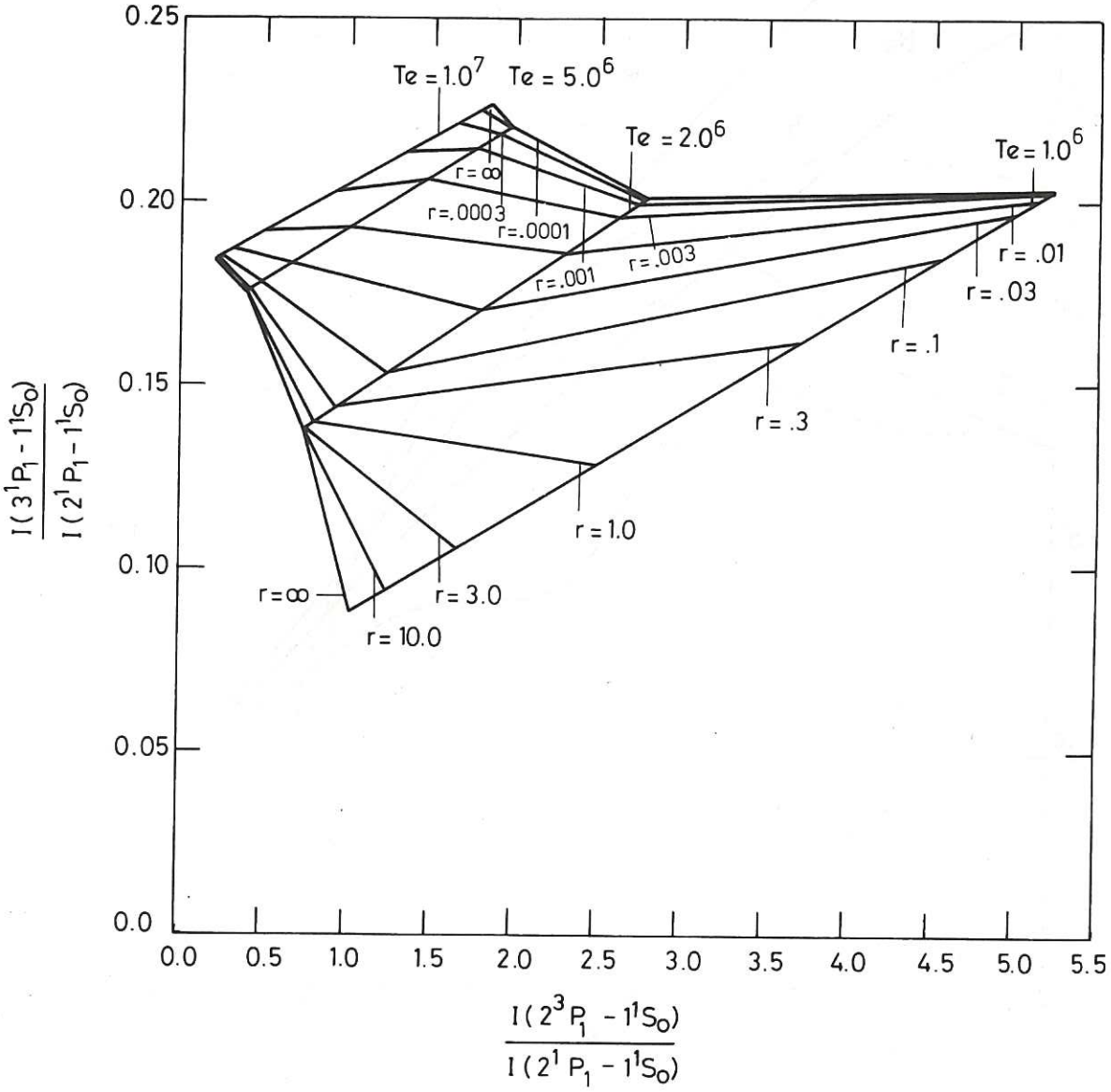

Fig.5 Te – r diagnostic plot. Ne = $1{\cdot}0^{13}$ cm^{-3}.

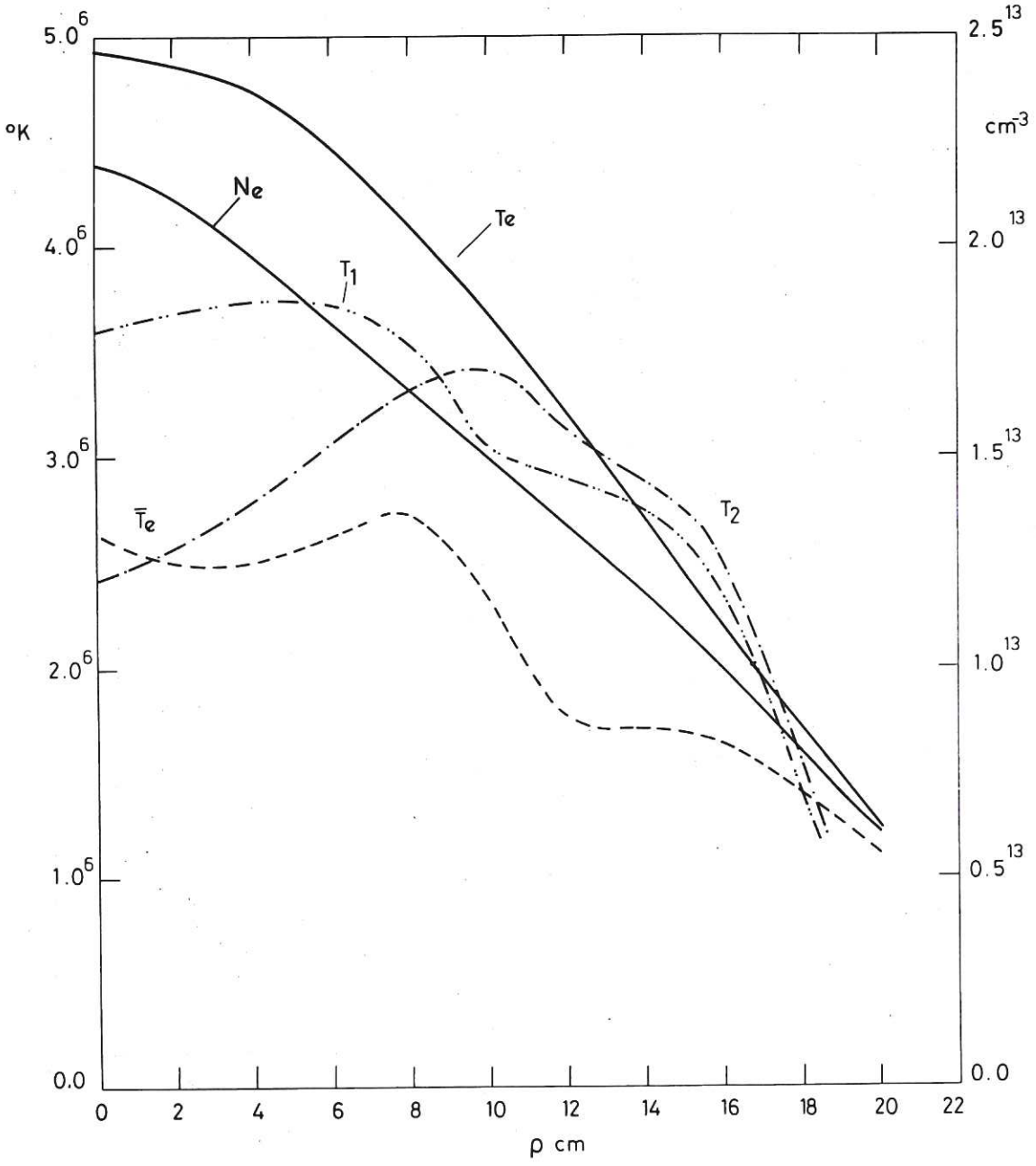

Fig.6 DITE. Electron temperature and electron density.
(Te, electron temperatures from Thomson scattering;
Ne, electron density from microwave phase shifts;
$\bar{T}e$, theoretically revised electron temperature;
T_1, single shot electron temperature at 60msec after start of current pulse;
T_2, single shot electron temperature at 120msec).

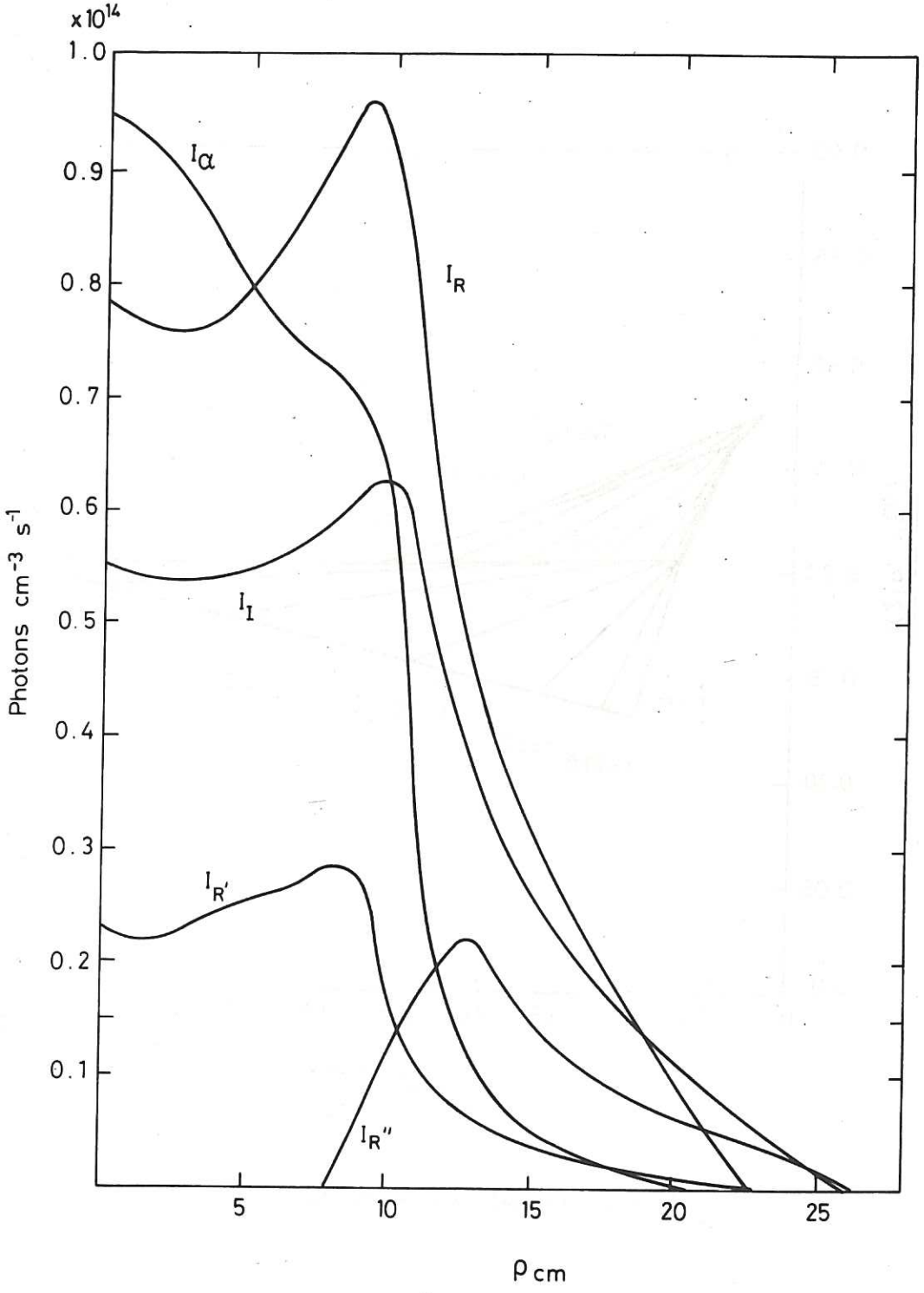

Fig.7 DITE. Abel inverted absolute emissivities. (I_R, $2^1P_1-1^1S_0$ for 0^{+6}; I_I, $2^3P_1-1^1S_0$ for 0^{+6}; $I_{R'}$, $3^1P_1-1^1S_0$ for 0^{+6}; I_α, 2^2P-1^2S for 0^{+7}; $I_{R''}$, 3^2P-2^2S for 0^{+5}.)

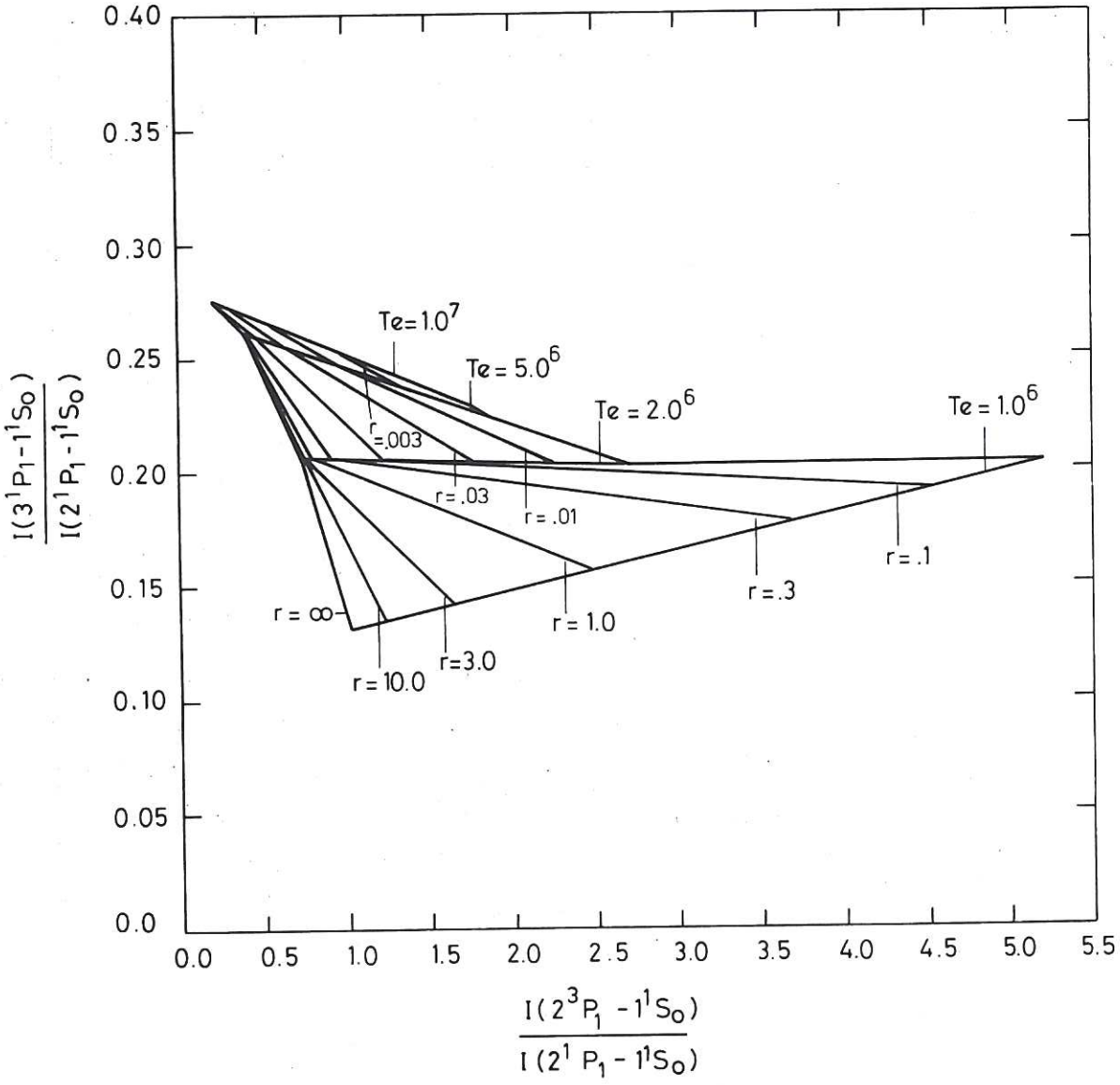

Fig.8 Te – r revised diagnostic plot. Ne = $1{\cdot}0^{13}$ cm^{-3}.

ρ	Ne	Te	I_R	I_I	I_α	U_R	V_R	U_I	V_I	n_1	n_2	n_1^*
0	2.19^{13}	4.92^{6}	7.75^{13}	5.50^{13}	1.38^{14}	1.44^{-23}	9.24^{-26}	3.35^{-20}	1.08^{-21}	2.37^{12}	5.91^{10}	2.08^{11}
2	2.11^{13}	4.85^{6}	7.57^{13}	5.40^{13}	0.95^{14}	1.41^{-23}	9.24^{-26}	3.28^{-20}	1.08^{-21}	2.43^{12}	6.09^{10}	1.52^{11}
4	1.98^{13}	4.73^{6}	7.75^{13}	5.41^{13}	0.82^{14}	1.37^{-23}	9.21^{-26}	3.32^{-20}	1.09^{-21}	2.38^{12}	7.06^{10}	1.45^{11}
6	1.81^{13}	4.43^{6}	8.36^{13}	5.59^{13}	0.75^{14}	1.24^{-23}	9.16^{-26}	3.13^{-20}	1.09^{-21}	2.41^{12}	9.45^{10}	1.59^{11}
8	1.66^{13}	4.10^{6}	9.29^{13}	5.96^{13}	0.73^{14}	1.11^{-23}	9.00^{-26}	3.00^{-20}	1.10^{-21}	2.22^{12}	1.35^{11}	1.90^{11}
10	1.49^{13}	3.69^{6}	8.74^{13}	6.27^{13}	0.59^{14}	1.05^{-23}	8.78^{-26}	2.71^{-20}	1.10^{-21}	3.47^{12}	1.40^{11}	2.06^{11}
12	1.33^{13}	3.21^{6}	5.20^{13}	4.40^{13}	1.75^{13}	7.12^{-24}	8.41^{-26}	2.30^{-20}	1.10^{-21}	2.61^{12}	1.35^{11}	8.80^{11}
14	1.18^{13}	2.68^{6}	3.57^{13}	3.00^{13}	0.71^{13}	4.77^{-24}	7.85^{-26}	1.76^{-20}	1.10^{-21}	1.55^{12}	1.67^{11}	6.02^{10}
16	1.00^{13}	2.18^{6}	2.57^{13}	2.20^{13}	0.39^{13}	2.74^{-24}	7.12^{-26}	1.14^{-20}	1.11^{-21}	9.02^{11}	2.60^{11}	6.78^{10}
18	7.90^{13}	1.71^{6}	1.72^{13}	1.63^{13}	0.20^{13}	1.21^{-24}	5.94^{-26}	5.82^{-21}	1.14^{-21}	6.64^{11}	5.11^{11}	1.04^{11}
20	6.05^{12}	1.25^{6}	0.96^{13}	1.13^{13}	0.10^{13}	3.01^{-25}	4.80^{-26}	1.67^{-21}	1.24^{-21}	7.33^{11}	1.48^{11}	3.01^{11}

Table 1: DITE. 0^{+7} and 0^{+6} derived stage abundances. (c.g.s. units)

ρ	Te	$(\frac{n_1}{n_2})$	$(\frac{n_1}{n_2})^{eq}$	$(\frac{\alpha_3}{\alpha_2})$	$(\frac{s_3 n_3}{\alpha_2 n_2})$	V_2	$\bar{T}e$	$(\frac{\bar{n}_1}{\bar{n}_2})$	$(\frac{\bar{n}_1}{\bar{n}_2})^{eq}$	$(\frac{\bar{\alpha}_3}{\bar{\alpha}_2})$	$(\frac{\bar{s}_3 \bar{n}_3}{\bar{\alpha}_2 \bar{n}_2})$	$\bar{V}_2$
0	4.92^{6}	4.02^{1}	8.40^{0}	1.10^{0}	4.55^{-2}	0	2.62^{6}	2.94^{0}	1.74^{0}	1.04^{0}	1.01^{-2}	0
2	4.85^{6}	4.00^{1}	8.07^{0}	1.10^{0}	4.53^{-2}	2.22^{3}	2.48^{6}	2.05^{0}	1.43^{0}	1.02^{0}	8.91^{-3}	-7.00^{0}
4	4.73^{6}	3.38^{1}	7.64^{0}	1.10^{0}	4.12^{-2}	3.67^{3}	2.50^{6}	1.67^{0}	1.49^{0}	1.02^{0}	8.74^{-3}	-5.38^{1}
6	4.43^{6}	2.55^{1}	6.62^{0}	1.11^{0}	6.50^{-2}	3.81^{3}	2.60^{6}	1.34^{0}	1.60^{0}	1.04^{0}	2.45^{-2}	-1.53^{2}
8	4.10^{6}	1.65^{1}	5.57^{0}	1.11^{0}	2.30^{-1}	3.18^{3}	2.72^{6}	1.07^{0}	1.96^{0}	1.06^{0}	8.53^{-2}	-1.99^{2}
10	3.69^{6}	2.47^{1}	4.37^{0}	1.12^{0}	1.52^{0}	3.87^{3}	2.32^{6}	1.02^{0}	1.15^{0}	9.84^{-1}	3.85^{-1}	-1.91^{2}
12	3.21^{6}	1.93^{1}	3.14^{0}	1.10^{0}	3.12^{0}	5.03^{3}	1.75^{6}	4.87^{-1}	3.60^{-1}	8.49^{-1}	4.47^{-1}	-1.28^{2}
14	2.86^{6}	9.32^{0}	1.84^{0}	1.05^{0}	2.31^{0}	4.37^{3}	1.70^{6}	3.13^{-1}	3.16^{-1}	8.34^{-1}	4.80^{-1}	-1.47^{2}
16	2.18^{6}	3.47^{0}	9.20^{-1}	9.51^{-1}	1.10^{0}	2.69^{3}	1.63^{6}	2.29^{-1}	2.54^{-1}	8.00^{-1}	3.67^{-1}	-1.48^{2}
18	1.71^{6}	1.30^{0}	3.14^{-1}	8.36^{-1}	5.12^{-1}	1.26^{3}	1.39^{6}	2.07^{-1}	1.04^{-1}	7.21^{-1}	1.88^{-1}	-1.52^{2}
20	1.25^{6}	4.96^{0}	5.31^{-2}	6.73^{-1}	1.51^{0}	4.04^{3}	1.12^{6}	2.03^{-1}	2.26^{-2}	5.93^{-1}	7.18^{-2}	-9.72^{1}

Table 2: DITE. 0^{+6} derived diffusion velocities (c.g.s. units)